Dynamics of transverse cloud rolls in the boundary layer with the Poiseuille shear flow

Cite as: Phys. Fluids **31**, 096601 (2019); https://doi.org/10.1063/1.5109523
Submitted: 09 May 2019 . Accepted: 12 August 2019 . Published Online: 03 September 2019

Quan Wang, and Chanh Kieu

Physics of Fluids ARTICLE scitation.org/journal/phf

Dynamics of transverse cloud rolls in the boundary layer with the Poiseuille shear flow

Cite as: Phys. Fluids 31, 096601 (2019); doi: 10.1063/1.5109523
Submitted: 9 May 2019 • Accepted: 12 August 2019 •
Published Online: 3 September 2019

Quan Wang[1,a)] and Chanh Kieu[2,b)]

AFFILIATIONS

[1] Department of Mathematics, Sichuan University, Chengdu 610065, China
[2] Department of Earth and Atmospheric Sciences, Indiana University, Bloomington, Indiana 47405, USA

[a)] Electronic mail: wqxihujunzi@126.com
[b)] Electronic mail: ckieu@indiana.edu

ABSTRACT

This study examines the formation of transverse cloud rolls associated with the Poiseuille shear flows that are occasionally observed in the Earth's atmospheric boundary layer. It is shown that the mechanisms underlying the formation of this type of transverse roll clouds can be explained in the framework of the transition dynamics and structural bifurcation for the incompressible flows. Specifically, the formation of transverse roll clouds is attributed to a subtle interaction between the vertical wind shear and the vertical temperature gradient in the atmospheric well-mixed boundary layer, which results in an attractor bifurcation and subsequent boundary layer separations. The topological structure of the Poiseuille shear flow at the boundary layer separation can be identified as transverse roll cloud.

I. INTRODUCTION

The Earth's atmosphere is essentially a multiscale fluid dynamical system. Due to its constant heat and moisture exchange with the Earth's surface, there are various types of convection that produce cloud patterns with different temporal and spatial scales, ranging from low-level stratus clouds to very high-level cirrus clouds. Because of the high similarity between the atmospheric convective cells and the Rayleigh-Bénard thermal convection, many analytical models have been proposed to understand the cloud patterns in the atmospheric boundary layer, based on the coupling of the Rayleigh-Bénard convection and a vertical shear flow such as the Couette flow or the Poiseuille flow.[1–12]

Among several types of low-level clouds, transverse cloud rolls (TCRs, also known as transverse bands or Arcus rolling clouds) whose convection axes are oriented perpendicular to their mean flow have occasionally been documented to develop near the top of the atmospheric planetary boundary layer (PBL).[2,13] Unlike the more common longitudinal convection rolls with cloud axes oriented roughly along the mean flow direction (also known as cloud streets),[11,12,14–17] TCRs are rare and relatively short-lived. Quite often, the existence of TCRs indicates the presence of a temperature inversion layer above the top of the boundary layer, which is favorable in the development of severe thunderstorm systems.

While TCRs are currently viewed as a form of the soliton of solitary waves propagating in the boundary layer, it is observed that TCRs share a similar structure with the transversal Rayleigh-Bénard convection embedded in a shear flow at a low Reynolds number.[4,18–24] Despite the dominant mode of longitudinal rolls in a strong shear flow, previous analytical, experimental, and modeling studies of the Rayleigh-Bénard thermal convection have shown that the transverse Rayleigh-Bénard cells can emerge in narrow bounded channels as a result of convective instability.[21–24] As discussed in the work of Muller *et al.*, the competition between the longitudinal and transversal rolls appears to be attributed to the lateral boundary conditions. Specifically, the preference of the transversal rolls is realized when the lateral sidewalls are included, whereas the longitudinal mode tends to always emerge prior to the transversal mode for an infinite domain. Regardless of the general dominance of longitudinal rolls, the similarity between TCRs and the transversal Rayleigh-Bénard convection in a low shear environment

suggests that TCRs may be examined beyond the current framework of linearized solitary waves.

It should be noted that although TCRs possess some similar features as the Rayleigh-Bénard-Poiseuille transversal rolls in laboratory experiments, the transverse rolls are observed only for a certain range of the vertical shear of mean flows and the Reynolds number.[21–24] In contrast, both numerical and experimental investigations on the Rayleigh-Bénard convection for the Couette and Poiseuille shear flows showed that the onset of instability responsible for longitudinal convection rolls is stationary at the high Reynolds number limit.[18–20,24] As a result, the longitudinal mode of cloud rolls seems to be more preferred in the atmospheric PBL and explains for the more frequent emergence of cloud streets. Such a dominance of the longitudinal rolls does not, however, preclude the existence of TCRs for which our current understanding about the underlying dynamics beyond the modeling and the linear stability framework is still limited.

Recent progress in the transition dynamics developed by Ma and Wang offers a potentially different framework to tackle the TCR formation from a different standpoint.[25–28] Specifically, they showed that with sufficiently strong vertical shear imposed on the zonal direction as well as a large vertical temperature gradient in the vertical direction, density differences in a fluid can generate intricate buoyancy-driven rolls that are manifested as boundary singularities aligned along the direction of the flow.[25–27,29] From this perspective, the well-known longitudinal cloud streets may be understood as a realization of the Rayleigh-Bénard convection along the mean flows, as discussed in Ref. 14. How this nonlinear dynamical mechanism can be applied to understand the formation of TCRs with the inclusion of diabatic heating associated with roll cloud formation has not been, however, explored.

Given previous results about the onset of TCRs that very much resembles the structural bifurcation and phase transition, it appears that the problem of the TCR formation can be examined from the perspective of the structural bifurcation theory and transition dynamics that we wish to explore in this study. An advantage of this transition theory is that one can study necessary conditions for the structural bifurcation to occur, from which we can analyze different types of transitions as well as the topological structure of flows beyond the classical linear stability framework. This approach has been demonstrated to be a promising tool for studying nonlinear dynamical transition phenomena such as Rayleigh-Bénard problems,[25,26] Taylor problems,[30] boundary layer separation,[31–33] and more recent applications in fluid dynamics.[27,34–37]

In this study, we wish to present a simplified model to understand the formation of TCRs from the perspective of Ma and Wang's transition dynamics. By including the effects of latent heat release associated with roll cloud formation, we will show that the TCR formation experiences two dynamical processes consisting of (1) an attractor bifurcation when the Rayleigh number is larger than a critical value and (2) a boundary layer separation behavior for some specific threshold of the vertical wind shear, thus offering different insights into the formation of transverse rolls.

II. A TRANSVERSE CLOUD ROLL MODEL

Given the structure of TCRs with their roll axes perpendicular to the mean shear flow (see Fig. 1), we adopt the Rayleigh-Bénard convection model with the Poiseuille shear to study the TCR formation.[25,38] Due to the complication of the latent heat release associated with roll cloud formation during the TCR development, the Rayleigh-Bénard convection model needs to be, however, modified to take into account the latent heating effects. Assuming the orientation of the TCR axes along the y-direction with the mean flows oriented in the x direction as shown in Fig. 1 such that the flow topology on each (x, z)-section exhibits same homogeneous structure in the y-direction (see Fig. 1), we introduce a modified Rayleigh-Bénard (hereinafter referred to as MRB) model under the Boussinesq approximation on the (x, z) plane as follows:

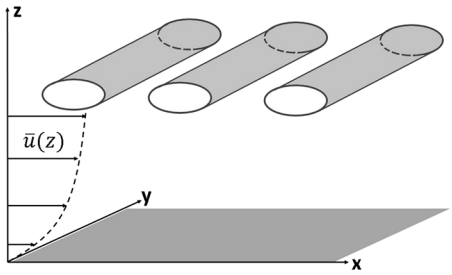

FIG. 1. A three-dimensional illustration of the transverse cloud roll model presented in this study, assuming the orientation of the cloud roll axes along the y-direction with a mean Poiseuille shear flow $\bar{u}(z)$ oriented in the x direction.

$$\begin{aligned}
\frac{Du}{Dt} &= -\frac{1}{\rho_0}\frac{\partial p}{\partial x} + \nu_E \Delta u,\\
\frac{Dw}{Dt} &= -\frac{1}{\rho_0}\frac{\partial p}{\partial z} + g\frac{\theta}{\theta_0} + \nu_E \Delta w,\\
\frac{D\theta}{Dt} &= Q + \kappa_E \Delta \theta,\\
\frac{\partial u}{\partial x} &+ \frac{\partial w}{\partial z} = 0,
\end{aligned} \tag{2.1}$$

where

$\mathbf{u} \equiv (u, w)$: velocity field in the (x, z) plane,
p : pressure field,
g : gravitational constant,
θ : potential temperature,
ν_E : turbulent eddy viscosity,
κ_E : thermal diffusion coefficient,
Q : diabatic heating associated with cloud roll formation,
θ_0 : a reference potential temperature at $z = 0$.

Note that in Eq. (2.1), $\frac{D}{Dt} = \frac{\partial}{\partial t} + (\mathbf{u}\cdot\nabla)$ is the material derivative, $(\mathbf{u}\cdot\nabla) = u\frac{\partial}{\partial x} + w\frac{\partial}{\partial z}$ denotes the advection operator, and $\Delta = \frac{\partial^2}{\partial x^2} + \frac{\partial^2}{\partial z^2}$ is the Laplacian operator. By definition, this MRB is defined on a rectangle domain as follows:

$$\Omega = [0, l] \times [0, h],$$

where l is the horizontal domain size and h is the vertical domain size. We note here the importance of a finite domain in this MRB

model for transverse cloud rolls as it reflects the fact that transverse rolls can only be realized for finite channels, as discussed in Refs. 22 and 24.

A quick inspection of the MRB model shows that this system admits a steady-state solution of the following form:

$$\begin{aligned} \bar{u}(z) &= -\frac{p_0 z^2}{2\rho_0 \nu_E} + \frac{h p_0}{\rho_0 \nu_E} z, \\ \bar{\theta}(z) &= \theta_0 - \frac{\theta_0 - \theta_1}{h} z, \\ \bar{w} &= 0, \end{aligned} \tag{2.2}$$

where $p_0 \equiv -\frac{\partial p}{\partial x}$ is the pressure gradient along the x direction and the overbar denotes the steady state. This steady-state solution is particularly simple if one considers a case in which the pressure gradient along the x direction is homogeneous such that $p_0 > 0$ is a positive constant. In this case, the mean flow $\bar{u}$ given in Eq. (2.2) would correspond to a shear flow with horizontal wind $\bar{u}$ quadratically increasing with height (see Fig. 2), while the potential temperature gradually decreases from a value θ_0 at $z = 0$ to θ_1 at $z = h$. The mean flow $\bar{u}(z)$ has an expected parabolic shape as it captures the Poiseuille shear for the transversal rolls.[16,17]

Due to the latent heating release associated with the TCR formation, it is necessary next to properly represent the latent heating effect in the MRB model. The full parameterization of the diabatic heating term Q to account for the cloud latent heat release would require a complete treatment of cloud microphysics, the moisture equation, as well as parameterizations of various cloud type properties and moments. These details of the cloud formation processes do not currently have any known analytical form that can be included in our model. Because of this complexity beyond the scope of our work, we present herein a simple closure for the diabatic heating effect by employing the following simplified parameterization for the diabatic heating term Q:

$$Q = \lambda w, \tag{2.3}$$

where λ is a proportional coefficient that governs the conversion of water phase transition. Given a typical vertical motion within the low-level cloud of 1–2 ms^{-1}, and corresponding changes in temperature in the order of 1–2 K h^{-1}, the value of this proportional constant $\lambda \sim 10^{-2}$ to 10^{-3} K m^{-1}. Physically, (2.3) states that stronger vertical motion would promote more cloud formation, thus resulting in larger latent heat release. Likewise, for descending motion, evaporative cooling will consume the ambient heat, thus decreasing potential temperature. While this diabatic heating parameterization is admittedly simple for the real atmospheric boundary layer, it could capture to some extent the main physical effects related to the cloud latent heating and will be hereinafter assumed. As will be seen later, it turns out that the main diabatic heating effect is to shift the stability threshold of the TCR formation but otherwise have little impacts on the transition dynamics processes.

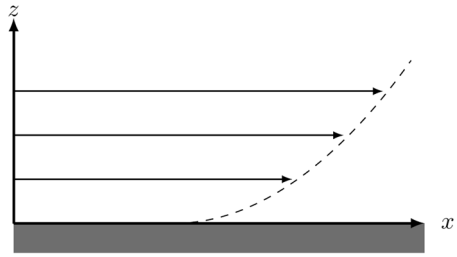

FIG. 2. Illustration of the topological structure of the mean flow as given by the steady state (2.2).

To close the system, the no-slip condition at the bottom boundary and the free condition at the top boundary will be assumed for the steady-state (2.2) such that

$$\bar{u} = 0 \text{ at } z = 0, \text{ and } \frac{\partial \bar{u}}{\partial z} = 0 \text{ at } z = h, \tag{2.4}$$

which are well approximated in real atmospheric conditions.

Remark. While the mean flow $\bar{u}$ given in (2.2) has the same expression as the Poiseuille flow, we stress that the mean flow (2.2) satisfies the free boundary condition at the top boundary $z = h$ instead of the nonslip condition at $z = h$ as for the Poiseuille flow (see Fig. 2). The free boundary at the top of the PBL is necessary so that the mean flow could approach the geostrophic wind in the free atmosphere as expected.

To study the stability and related bifurcation of the mean flow (2.2), we divide the total fields into the mean $(\bar{\mathbf{u}}, \bar{\theta})$ and the perturbation component $(\mathbf{u}', \theta')$ as follows:

$$\mathbf{u} = \bar{\mathbf{u}} + \mathbf{u}', \quad \theta = \theta_0 + \theta'. \tag{2.5}$$

Unlike the traditional linear stability analyses that always assume $\mathbf{u}' \ll \bar{\mathbf{u}}$ such that a linearization can be carried out, we emphasize that our partition (2.5) does not require this linearization. As will be seen in the subsequent analyses on the central manifold, all nonlinear terms will be retained for our stability analyses on the central manifold as discussed in Ref. 27.

Upon substituting this partition into the governing equation (2.1) and neglecting primes for the sake of notation, the MRB system for the perturbations is obtained as

$$\begin{aligned} &\frac{Du}{Dt} + \bar{u}\frac{\partial u}{\partial x} + w\frac{d\bar{u}}{dz} = \nu_E \Delta u - \frac{1}{\rho_0}\frac{\partial p}{\partial x}, \\ &\frac{Dw}{Dt} + \bar{u}\frac{\partial w}{\partial x} = \nu_E \Delta w - \frac{1}{\rho_0}\frac{\partial p}{\partial z} + g\frac{\theta}{\theta_0}, \\ &\frac{D\theta}{Dt} + \bar{u}\frac{\partial \theta}{\partial x} = \kappa_E \Delta \theta + \frac{(\theta_0 - \theta_1 + H\lambda)}{H} w, \\ &\frac{\partial u}{\partial x} + \frac{\partial w}{\partial z} = 0. \end{aligned} \tag{2.6}$$

Introduce next a set of the following to nondimensionalize the MRB system:

$$\begin{aligned} &t = \frac{h^2}{\kappa_E} t^*, \quad (x, z) = h(x^*, z^*), p = \rho_0 \frac{\kappa_E^2}{h^2} p^*, \\ &\mathbf{u} = \frac{\kappa_E}{H}\mathbf{u}^*, \quad \theta = (\theta_0 - \theta_1)\theta^*, \end{aligned} \tag{2.7}$$

where the asterisk denotes nondimensionalized variables. Substituting these nondimensional variables into (2.6) and hereinafter again neglecting the asterisk for all variables for convenience, we obtain

$$\begin{aligned}
&\frac{Du}{Dt} + \beta f(z)\frac{\partial u}{\partial x} + \beta f'(z)w = P_r\Delta u - \frac{\partial p}{\partial x},\\
&\frac{Dw}{Dt} + \beta f(z)\frac{\partial w}{\partial x} = P_r\Delta w - \frac{\partial p}{\partial z} + P_r\hat{R}\theta,\\
&\frac{D\theta}{Dt} + \beta f(z)\frac{\partial \theta}{\partial x} = \Delta\theta + (1+\bar{\lambda})w,\\
&\frac{\partial u}{\partial x} + \frac{\partial w}{\partial z} = 0,
\end{aligned} \tag{2.8}$$

where

$$f(z) = \left(z - \frac{z^2}{2}\right), \tag{2.9}$$

and $\hat{R} = \frac{g(\theta_0-\theta_1)h^3}{\theta_0\nu_E\kappa_E}$ is the Rayleigh number, $\bar{\lambda} = \frac{h\lambda}{\theta_0-\theta_1}$ is a nondimensional number related to the latent diabatic heating (hereinafter referred to as the diabatic parameter), $P_r = \frac{\nu_E}{\kappa_E}$ is the Prandtl number, and $\beta = \frac{p_0h^3}{\rho_0\nu_E\kappa_E}$ is a nondimensional parameter encoding the strength of the Poiseuille shear, the pressure gradient of the mean flow p_0, and the contribution from the eddy viscosity. While both Rayleigh and β numbers depend inversely on the eddy viscosity ν_E and diffusion κ_E, these two numbers have different physical implications. Specifically, the effect of the vertical temperature gradient is contained only in the Rayleigh number, whereas the effect of the horizontal wind shear of the mean flows is contained in the β number. For a typical atmospheric PBL, the Rayleigh number varies in the range of 10–10^3, and the β number varies in the range of 10^{-2} to 1. Depending on the values of these two numbers, the MRB could possess different dynamical behaviors as will be shown below.

To simplify our analyses, let us make the transformation $\theta \to \sqrt{\frac{1+\bar{\lambda}}{\hat{R}}}\theta$ in the nondimensional MRB system (2.8) to obtain

$$\begin{aligned}
&\frac{Du}{Dt} + \beta f(z)\frac{\partial u}{\partial x} + \beta f'(z)w = P_r\Delta u - \frac{\partial p}{\partial x},\\
&\frac{Dw}{Dt} + \beta f(z)\frac{\partial w}{\partial x} = P_r\Delta w - \frac{\partial p}{\partial z} + P_r\sqrt{R}\theta,\\
&\frac{D\theta}{Dt} + \beta f(z)\frac{\partial \theta}{\partial x} = \Delta\theta + \sqrt{R}w,\\
&\frac{\partial u}{\partial x} + \frac{\partial w}{\partial z} = 0,
\end{aligned} \tag{2.10}$$

where a modified Rayleigh number R is now defined as

$$R = \hat{R}(1+\bar{\lambda}). \tag{2.11}$$

An important observation in the new system (2.10) is that the modified Rayleigh number R is now the key parameter governing the transition dynamics, which incorporates both the classical Rayleigh number and the latent heating effect via the diabatic parameter $\bar{\lambda}$. The transformation $\theta \to \sqrt{\frac{1+\bar{\lambda}}{\hat{R}}}\theta$ is thus significant because it can combine both the Rayleigh number $\hat{R}$ and the diabatic parameter $\bar{\lambda}$ into a single control parameter R in the system (2.10). Such a reduction thus allows us to drastically simplify our discussion and stability analyses. The system (2.10) will be hereinafter referred to as the nondimensional MRB model for our analyses of the transversal rolls, in which R is the model control parameter. In these coordinates, the model domain for Eq. (2.10) now becomes

$$\Omega = [0,\gamma]\times[0,1], \quad \gamma = l/h, \tag{2.12}$$

and the corresponding boundary conditions for the perturbations are reduced to

$$\begin{aligned}
&u = 0, \quad \frac{\partial w}{\partial x} = \frac{\partial \theta}{\partial x} = 0, \quad x = 0,\gamma,\\
&w = 0, \quad z = 0,1;\\
&u = 0, \quad z = 0; \quad \frac{\partial u}{\partial z} = 0, \quad z = 1;\\
&\theta = 0, \quad z = 0,1.
\end{aligned} \tag{2.13}$$

Remark. For the turbulent Prandtl number P_r, it will be assumed herein that $P_r \approx 1$ as in previous studies of the atmospheric PBL turbulence.[39,40] *Because $P_r = 1$, the thermal eddy viscosity coefficient κ_E will be therefore the same as ν_E. In a typical atmospheric boundary layer, it should be noted that the eddy viscosity coefficient ν_E varies in a wide range of 10–10^5 m^2 s^{-1}, depending on the mean flows, stratification, and surface type in the PBL. For the specific setting of transversal rolls that this study focuses on, we will consider a relatively large value $\nu_E = 1000$ m^2 s^{-1} for both the vertical and horizontal eddy coefficients in a well-mixed PBL. This large value of the eddy viscosity can happen when the mean flow $\bar{u}$ varies sufficiently slowly with height in the PBL, which is permissible in the well-mixed boundary layer.*

A. First eigenvalue and eigenvector analyses

Following the standard procedure in transition dynamics, we consider first the eigenvalue problem for the linear operator in the MRB system (2.10) as follows:

$$\begin{aligned}
&P_r\Delta u - \beta f(z)\frac{\partial u}{\partial x} + \beta f'(z)w - \frac{\partial p}{\partial x} = \eta u,\\
&P_r\Delta w - \beta f(z)\frac{\partial w}{\partial x} - \frac{\partial p}{\partial z} + P_r\sqrt{R}\theta = \eta w,\\
&\Delta\theta - \beta f(z)\frac{\partial \theta}{\partial x} + \sqrt{R}w = \eta\theta,\\
&\frac{\partial u}{\partial x} + \frac{\partial w}{\partial z} = 0,
\end{aligned} \tag{2.14}$$

whose boundary conditions are given by (2.13) and η is an eigenvalue. The corresponding dual eigenvalue system for Eq. (2.14) is given as follows:

$$\begin{aligned}
&P_r\Delta u^* + \beta f(z)\frac{\partial u^*}{\partial x} - \frac{\partial p}{\partial x} = \eta u^*,\\
&P_r\Delta w^* + \beta f(z)\frac{\partial w^*}{\partial x} + \beta f'(z)u^* - \frac{\partial p}{\partial z} + \sqrt{R}\theta^* = \eta w^*,\\
&\Delta\theta^* + \beta f(z)\frac{\partial \theta^*}{\partial x} + P_r\sqrt{R}w^* = \eta\theta^*,\\
&\frac{\partial u^*}{\partial x} + \frac{\partial w^*}{\partial z} = 0.
\end{aligned} \tag{2.15}$$

The solution (u^*, w^*, θ^*) to the dual system (2.15) will be used to normalize the eigenvector (u, w, θ) by the identity

$$\int_0^\gamma \int_0^1 \left(uu^* + ww^* + \theta\theta^*\right) dx\, dz = 1.$$

The analyses of Eq. (2.14) will be significantly simplified if we note that for a typical PBL depth, $h \sim 1000$ m, $\rho_0 \sim 1$ kg m^{-3} and

$p_0 \sim 10^{-4}$ Pa m^{-1}. It is then easy to see that the β number is ~0.1. Such a small value of β implies that the vertical wind shear of the mean flow must not be too strong, which is viewed as a requirement for transverse cloud rolls in our MRB model. Mathematically, a small β number is noteworthy because it allows us to consider the contribution of β-related terms as a high-order contribution superimposed on Eq. (2.10). With $\beta \sim 0.1 \ll 1$, it is technically possible to treat the MRB system with $\beta = 0$ as a zero-order approximation (i.e., no vertical wind shear) on which the nonlinear contribution related to $\beta \neq 0$ can be imposed. For $\beta = 0$, the first eigenvector of the linear differential operator in (2.14) then satisfies

$$\begin{aligned} &P_r\Delta u - \frac{\partial p}{\partial x} = 0,\\ &P_r\Delta w - \frac{\partial p}{\partial z} + P_r\sqrt{R}\theta = 0,\\ &\Delta\theta + \sqrt{R}w = 0,\\ &\frac{\partial u}{\partial x} + \frac{\partial w}{\partial z} = 0. \end{aligned} \tag{2.16}$$

We note that the *first* eigenvector is defined in the sense of an eigenvector that corresponds to the largest eigenvalue of the linear Laplacian operator in (2.14). Because the spectrum of eigenvalues of the Laplacian operator with a positive forcing is negative, the largest first eigenvalue is therefore zero, i.e., $\eta_1 = 0$.

It can now be seen directly from Eq. (2.16) that the zero-order approximation with $\beta = 0$ is nothing but the classical Rayleigh-Bénard thermal convection in the absence of the vertical wind shear, which has extensively been studied in previous studies. As presented in Ref. 4, the first eigenvector of (2.16) has the following form:

$$\begin{aligned} u(x,z) &= \frac{1}{a_k}\sin a_k x U'(z),\\ w(x,z) &= -\cos a_k x U(z),\\ \theta(x,z) &= -\frac{1}{a_k^2\sqrt{R_c}}\cos ax\left(\frac{d^2}{dz^2} - a_k^2\right)^2 U(z), \end{aligned} \tag{2.17}$$

where $a_k = \frac{k\pi}{\gamma}$, R_c is the critical value of R above which the system (2.16) will possess the first positive eigenvalue, and $U(z)$ is a function of z that satisfies the following equation:

$$\begin{aligned} &\left(\frac{d^2}{dz^2} - a_k^2\right)^3 U = -a_k^2 R_0 U,\\ &U = \left(\frac{d^2}{dz^2} - a_k^2\right)^2 U = 0, \text{ at } z = 0, 1\\ &U' = 0 \text{ at } z = 0; U'' = 0 \text{ at } z = 1. \end{aligned} \tag{2.18}$$

In the explicit form, the function $U(z)$ can be expressed as[4]

$$\begin{aligned} U(z) &= \sin A_0\left(\frac{z}{2} - \frac{1}{2}\right) - f_1(z) + f_2(z),\\ f_1(z) &= B_1 \sinh A_1\left(\frac{z}{2} - \frac{1}{2}\right)\cos A_2\left(\frac{z}{2} - \frac{1}{2}\right),\\ f_2(z) &= B_2 \cosh A_1\left(\frac{z}{2} - \frac{1}{2}\right)\sin A_2\left(\frac{z}{2} - \frac{1}{2}\right), \end{aligned} \tag{2.19}$$

where A_0, A_1, B_1, and B_2 are constants given by

$$\begin{aligned} &A_0 = 7.137\,877, A_1 = 9.110\,819, A_2 = 3.789\,300,\\ &B_1 = 0.017\,073\,89, B_2 = 0.003\,456\,45. \end{aligned} \tag{2.20}$$

Note that in the above expression for $U(z)$, R_c is not a free parameter but is a critical Rayleigh number that is determined by the scale ratio of the domain γ and boundary conditions. More precisely, once γ is specified, there must exist a value k such that $\frac{k\pi}{\gamma}$ is consistent with R_c as obtained from Eq. (2.18) and the boundary condition. Indeed, a direct estimation of the eigenvalue of (2.16) shows that k is proportional to γ, i.e., for each γ, k will be determined by

$$\left|\frac{k\pi}{\gamma} - 2.682\right| = \min_{n\in\mathbb{N}}\left|\frac{n\pi}{\gamma} - 2.682\right|, \tag{2.21}$$

where the value 2.682 is derived from the boundary conditions (2.13) as calculated in the work of Chandrasekhar.[4] It is also seen from the above expression of R_c that the first eigenvalue R_c of (2.16) is simple, except for some discrete values of the aspect ratio $\gamma = \gamma_k$.[4]

We observe next another special property of the linear system (2.16) in the absence of vertical wind shear (i.e., $\beta = 0$) that the flow field is always nondivergent (i.e., $\nabla\cdot\mathbf{u} = 0$). As such, the value R_c can be considered as an eigenvalue of the linear system (2.16) under the Leray projection. This observation is important as it allows us to treat R_c as a limit of the more general eigenvalue of the linear system (2.14). Indeed, denote the first eigenvalue of (2.14) as R_c^β for $\beta \neq 0$; we then have

$$\lim_{\beta\to 0} R_c^\beta = R_c. \tag{2.22}$$

In Sec. II B, we will use this property and examine the attractor bifurcation of the mean flow (2.2) as the two numbers R, β vary under the condition that $\beta \ll 1$.

B. Attractor bifurcation

As shown in Ref. 27, the classical Rayleigh-Bénard convection problem possesses an attractor bifurcation for a given critical Rayleigh number R_c. Following Ma and Wang,[27] we will show in this section that the MRB model does possess a very similar property, even when the latent heating and the vertical wind shear of the mean flows are included. To this end, let us define functional spaces H and H_1 as follows:

$$H = \left\{(\mathbf{u},\theta) \in L^2(\Omega)^3 | \nabla\cdot\mathbf{u} = 0\right\}, \tag{2.23}$$

$$H_1 = \left\{(\mathbf{u},\theta) \in H^2(\Omega)^3\right\} \bigcap H, \tag{2.24}$$

where $(\mathbf{u}, \theta)$ satisfy the boundary conditions (2.13), and define the operators L_R, S_β, and G on the space H_1 as follows:

$$\begin{aligned} L_R &= A + \sqrt{R}B,\\ A\mathbf{v} &= (\mathbb{P}[P_r\Delta u, P_r\Delta w], \theta),\\ B\mathbf{v} &= [\mathbb{P}(0, P_r\theta), w],\\ S_\beta\mathbf{v} &= \left(\mathbb{P}\left[-\beta(z - \frac{z^2}{2})\frac{\partial u}{\partial x} - \beta(1-z)w, -\beta(z-\frac{z^2}{2})\frac{\partial w}{\partial x}\right],\right.\\ &\qquad \left.-\beta(z-\frac{z^2}{2})\frac{\partial\theta}{\partial x}\right),\\ G(\mathbf{v},\mathbf{v}) &= -(\mathbb{P}[(\mathbf{u}\cdot\nabla)u, (\mathbf{u}\cdot\nabla)w], (\mathbf{u}\cdot\nabla)\theta), \end{aligned} \tag{2.25}$$

in which $\mathbb{P}$ is the Leray projection. Equation (2.10) is then rewritten in the form of an operator equation as follows:

$$\frac{d\mathbf{v}}{dt} = L_R\mathbf{v} + S_\beta\mathbf{v} + G(\mathbf{v}), \text{where } \mathbf{v} \equiv (u, w, \theta). \tag{2.26}$$

Let the parameters (λ, ε) in Ma and Wang's boundary layer separation theorem[27] correspond to (R, β) in our MRB system, a direct verification of the above operators shows that L_R, S_β, and G satisfy the attractor bifurcation conditions. Furthermore, L_R is symmetric and

$$\big(G(\mathbf{v}, \mathbf{v}^*), \mathbf{v}^*\big) = 0,$$

where $G(\mathbf{v}, \mathbf{v}^*)$ is defined from (A5) as

$$G(\mathbf{v}, \mathbf{v}^*) = -\big(P_L\big((\mathbf{u}\cdot\nabla)u^*, (\mathbf{u}\cdot\nabla)w^*\big), (\mathbf{u}\cdot\nabla)\theta^*\big).$$

Because it is known from the results in Refs. 25 and 38 that $\mathbf{0}$ is an asymptotically stable steady state of the linear part of the equation

$$\frac{d\mathbf{v}}{dt} = L_R\mathbf{v} + G(\mathbf{v})$$

at $R = R_c$ in the absence of vertical wind shear, the MRB system (2.10) satisfies all conditions in Ref. 27. As a result, we have the following two important theorems concerning the attractor bifurcation of the general MRB system in the presence of $\beta \neq 0$.

Theorem II.1. *There exists a positive number β^* such that for any $|\beta| < \beta^*$, the MRB system (2.10) with the boundary conditions (2.13) undergoes a continuous transition at $(\mathbf{u}, \theta, R) = (\mathbf{0}, 0, R_c^\beta)$. Furthermore, the following results hold true:*

(1) *There is a neighborhood $U \subset H$ of $(\mathbf{u}, \theta) = (\mathbf{0}, 0)$ such that the system (2.10) bifurcates to an attractor $\Sigma_R^\beta \subset U$ for $R > R_c^\beta$ with $\mathbf{0} \notin \Sigma_R^\beta$, which attracts $U\backslash\Gamma$, where Γ is the stable manifold of $(\mathbf{u}, \theta) = (\mathbf{0}, 0)$ with codimension m $(1 \le m \le 2)$. Besides, the dimension of Σ_R^β is either zero or one.*

(2) *Each $\mathbf{v}_R \in \Sigma_R^\beta$ can be expressed in the form of*

$$\mathbf{v}_R = \mathbf{v}_{R,1}^0 + \mathbf{w}_R^\beta, \quad \lim_{\beta\to 0} \|\mathbf{w}_R^\beta\|/\|\mathbf{v}_{R,1}^0\| = 0,$$

where $\mathbf{v}_{R,1}^0 = (u, w, \theta)$ is the first eigenvector of Eq. (2.16) *given by (2.17).*

Theorem II.2. *Under the conditions of above theorem, if $\gamma \neq \gamma_k$, then the attractor Σ_R^β of (2.26) bifurcated from $(\mathbf{u}, \theta, R) = (\mathbf{0}, 0, R_c^\beta)$ consists of two states, expressed in the form of*

$$\begin{aligned} \Sigma_R^\beta &= \{\mathbf{u}_{R,1}^\beta, \mathbf{u}_{R,2}^\beta\}, \\ \mathbf{u}_{R,1}^\beta &= a_1(R,\beta)\mathbf{v}_{R,1}^0 + o(|a_1(R,\beta)|), \\ \mathbf{u}_{R,2}^\beta &= -a_2(R,\beta)\mathbf{v}_{R,1}^0 + o(|a_i(R,\beta)|). \end{aligned} \tag{2.27}$$

Furthermore, the coefficients in (2.27) are given as follows:

$$a_1 = \frac{\sqrt{b^2(\beta) + 4a(R,\beta)} - |b(\beta)|}{2c(\beta)} + o(|b|, |\beta|),$$

$$a_2 = \frac{\sqrt{b^2(\beta) + 4a(R,\beta)} + |b(\beta)|}{2c(\beta)} + o(|b|, |\beta|),$$

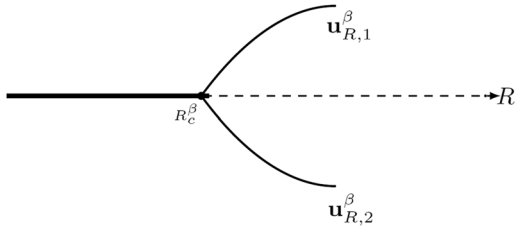

FIG. 3. The topological structure of the attractor bifurcating at the critical Rayleigh number R_c^β as the modified Rayleigh number R varies.

where

$$\begin{aligned} a(R,\beta) &= \sigma(\beta)(R - R_c^\beta) + o(R,\beta), \\ \sigma(\beta) &= \eta_1'\big(R_c^\beta\big)c(\beta), \\ c(\beta) &= \int_\Omega (\mathbf{v}_{R,1}^\beta\cdot\nabla)\Phi_2\cdot\mathbf{v}_{R,1}^{\beta,*}\,dxdz + \int_\Omega (\Phi_2\cdot\nabla)\mathbf{v}_{R,1}^\beta\cdot\mathbf{v}_{R,1}^{\beta,*}\,dxdz, \\ b(\beta) &= -\int_\Omega (\mathbf{v}_{R,1}^\beta\cdot\nabla)\mathbf{v}_{R,1}^\beta\cdot\mathbf{v}_{R,1}^{\beta,*}\,dxdz, \end{aligned}$$

where $\mathbf{v}_{R,1}^\beta = (u_{R,1}^\beta, w_{R,1}^\beta, T_{R,1}^\beta)$ is the first eigenvector determined by (2.14), $\eta_1' = 0$ is the first-order derivative of the first eigenvalue determined by (2.14) with respect to the R, $\mathbf{v}_{R,1}^{\beta,*}$ solving Eq. (2.15) *is the dual eigenvector associated with the $\mathbf{v}_{R,1}^\beta$, and Φ_2 solves the equation $L_R\Phi_2 = -(\mathbf{v}_{R,1}^\beta\cdot\nabla)\mathbf{v}_{R,1}^\beta$ in which the operator L_R defined in (A5). In addition, the topological structure of the attractor bifurcation Σ_R^β is shown in Fig. 3.*

The bifurcation diagram shown in Fig. 3 for the perturbation flow $\mathbf{u}$ is especially interesting because it indicates that there now emerge two new stable states $\mathbf{u}_{R,1}^\beta$ and $\mathbf{u}_{R,2}^\beta$ corresponding to the clockwise and counterclockwise orientation of perturbation flows when $R > R_\beta^c$, even in the presence of vertical wind shear (i.e., $\beta \neq 0$, see Fig. 4 for an example of the clockwise orientation solution $\mathbf{u}_{R,1}^\beta$). While the modified Rayleigh number R is now proportional to the Rayleigh number $\hat{R}$ and the diabatic parameter λ, the bifurcation diagram for the MRB model (2.6) with the effect of latent heating included in the parameter λ is still the same when λ varies. In this

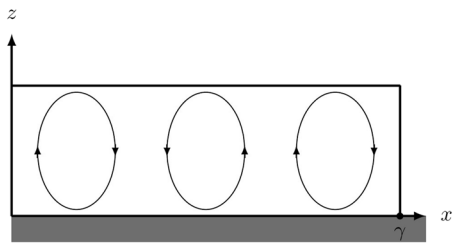

FIG. 4. Illustration of the topological structure of flows associated with the bifurcated solution for $\mathbf{u}_{R,1}^\beta$ with $k = 3$ in (2.17). The other solution $\mathbf{u}_{R,2}^\beta$ is similar but with opposite flow orientation.

regard, the main effect of the latent heating on the attractor bifurcation is to allow for the bifurcation to take place earlier than that without latent heating (i.e., the actual Rayleigh number $\hat{R}$ is smaller). In this regard, the effect of the latent heating via parameter λ is to destabilize the steady-state (2.2) and results in a new transitioned state, even when the Rayleigh number $\hat{R}$ is still below the critical value R_c.

III. BOUNDARY LAYER SEPARATION

Theorems II.1 and II.2 presented in Sec. II B provide some formal conditions for which an attractor bifurcation of the perturbations (u, w, θ) occurs as well as the new stable structure $\mathbf{u}^{\beta}_{R,1}$ and $\mathbf{u}^{\beta}_{R,2}$ of the perturbation flows. In the absence of the vertical wind shear (i.e., $\beta = 0$), these clockwise or counterclockwise convective rolls within the PBL could alone offer some picture of TCRs if one notes that the ascending branch between two rolls, as shown in Fig. 4, is where the cloud is expected to form along the rolls. The distance between the transverse cloud bands is therefore roughly the diameter of the convective rolls illustrated in Fig. 4.

The presence of vertical shear (i.e., $\beta \neq 0$) introduces, however, a new type of behavior, the so-called boundary layer separation. To illustrate this potentially new behavior, Fig. 5 shows the total flow field $(u, w)^T = (\bar{u}, 0)^T + \mathbf{u}^{\beta}_{R,i}$ $(i = 1, 2)$ after the attractor bifurcation for the case $\beta \neq 0$. Similar to the classical boundary layer separation of flows around a curve surface, there is potentially a stagnation point due to the cancellation of the mean and the perturbation flows near the surface, where the flows must ascend due to the incompressibility of the fluid and nonpenetrable surface boundary. The emergence of these boundary layer separation points may account for the formation of a string of transverse cloud rolls. In this section, we will apply the results obtained by Refs. 38, 41, and 42 for the boundary layer separation of shear flows in the presence of latent heating convection to understand further the formation of transverse cloud rolls.

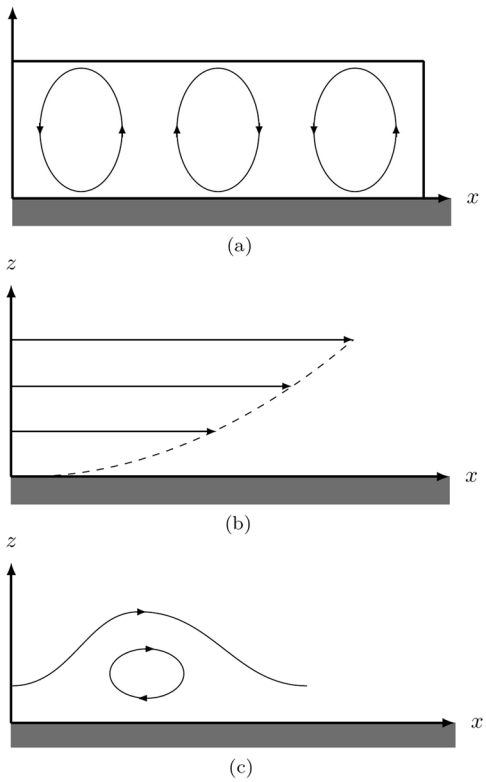

FIG. 5. Illustration of (a) the new stable perturbation flow $\mathbf{u}_{R,1}$ after the attractor bifurcation, (b) the mean shear flow $\bar{u}$, and (c) the total flow $(\bar{u}, 0) + \mathbf{u}^{\beta}_{R,1}$ that experiences a boundary layer separation if β is sufficiently small and $R > R^{\beta}_c$ increases.

To this end, we will first introduce a formal definition of the boundary layer separation for our subsequent analyses. Let Ω be a bounded and open domain of R^2. $\partial\Omega$ is C^{r+1}. $T\Omega$ is a tangent bundle of Ω. $C^r(T\Omega)$ is the space of all C^r fields on R^2,

$$B^r_0(T\Omega) = \{\mathbf{u} \in C^r(T\Omega) | \nabla \cdot \mathbf{u} = 0, \mathbf{u}|_{\partial\Omega} = 0\},$$

where $\mathbf{n}$ and τ are the unit normal and tangent vectors of $\partial\Omega$, respectively. We follow Refs. 43 and 44 and define the *boundary layer separation* as follows:

Definition III.1. In a neighborhood of $\tilde{x} \in \partial\Omega$, *assume that* $\mathbf{u}(x, t)$ *is topologically equivalent to the flow structure, as shown in* Fig. 6(a) *for* $t < t_0$, but it is topologically equivalent to the flow structure, as shown in Fig. 6(b) for $t > t_0$. In this case, we state that the flow field $\mathbf{u} \in C^1([0, T]; B^2_0(T\Omega))$ possesses a boundary layer separation at $(t_0, \tilde{x})$.

With the above definition and Theorem II.2, we have the following result:

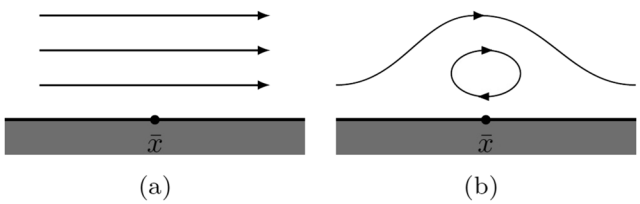

FIG. 6. Illustration of the total flow for (a) before the boundary layer separation and (b) after the boundary layer separation for which a new total flow structure develops at the location $\tilde{x}$.

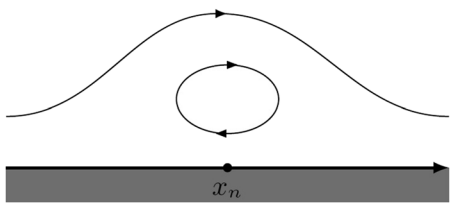

FIG. 7. Illustration of the development of a vortex separated from the boundary due to the emergence of boundary singularity at the location $(x_n, 0)$.

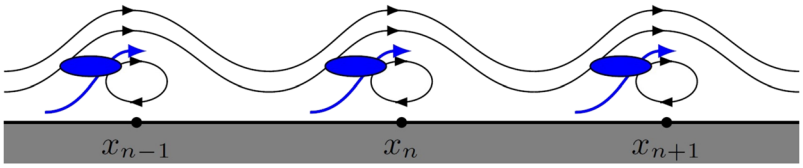

FIG. 8. A topological structure of the flow after multiple boundary layer separation events take place along the x-direction, which are identified as the locations of transverse roll clouds. Blue arrows denote the ascending branches developed as a result of the boundary layer separation. Transverse cloud rolls form along these branches, which are denoted by blue ovals.

Theorem III.1. *There exists β_0 such that for any $0 < \beta < \beta_0$, the following assertions hold true for the two solutions $\mathbf{v}_{R,i} = (\bar{u}, 0) + \mathbf{u}^{\beta}_{R,i}(i = 1, 2)$, where $\mathbf{u}^{\beta}_{R,i}$ given in Theorem II.2:*

(1) *For $\mathbf{v}_{R,1}$, there is $R_1 > R_c^{\beta}$ such that for $R_c^{\beta} < R < R_1$, its topological structure is equivalent to the shear flow $(\bar{u}, 0)$ shown in Fig. 2, while for $R > R_1$, there is a unique vortex separated from each boundary singular point $(x_n, 0) \in \partial\Omega$, shown in Fig. 7, where x_n is approximately given by*

$$x_n = \frac{(4n+1)\pi}{2a_k}.$$

(2) *For $\mathbf{v}_{R,2}$, there exists a positive number $b_0 > 0$ such that only one of the following results holds true:*

i. *If $b(\beta) < b_0$, there exists $R_2 > R_c^{\beta}$ such that for $R_c^{\beta} < R < R_2$, vector field $\mathbf{v}_{R,2}$ has the topological structure similar to $(\bar{u}, 0)$ shown in Fig. 2, while for $R > R_2$, there is a unique vortex separated from each boundary singular point $(x_n, 0) \in \partial\Omega$ of $\mathbf{v}_{R,2}$, shown in Fig. 7, where x_n is approximately given by, respectively,*

$$x_n = \frac{(4n+1)\pi}{2a_k}.$$

ii. *If $b(\beta) > b_0$, then for $R > R_c^{\beta}$, its topological structure is equivalent to that given in Fig. 8.*

(3) *There exists $R_3 > R_i (i = 1, 2)$ such that for $R_i (i = 1, 2) < R < R_3$, the topological structure of $\mathbf{v}_{R,i}$ is shown in Fig. 8.*

Proof. The proof can be found in the Appendix. □

As seen in the above of Theorem III.1, the existence of the mean shear $\bar{u}$ is critical for the development of the boundary layer separation. Without the vertical shear of the mean flow (i.e., $\beta = 0$), Theorem II.2 implies then that the dynamical process is simply a direct transition from the rest state to a set of traditional Rayleigh-Bénard convection cells, and so no boundary layer separation could develop. Note also in Theorem III.1 that the upper bounds R_1 and R_2 are required to ensure the topological flow structure, as shown in Fig. 8. In fact, for $R \gg R_2$, there may appear a new type of convective rolls between two consecutive locations x_n and x_{n+1} near $z = 1$ that do not share any similarity to TCRs. Thus, the requirement for R_i $(i = 1, 2)$ in Theorem III.1 is necessary.

IV. DISCUSSIONS

From the mathematical perspective, the attractor bifurcation and the related boundary layer separation in the MRB system in the presence of vertical wind shear as dictated by Theorems II.1–III.1 are promising for the TCR formation problem. This is because these theorems offer a different picture of the dynamical mechanisms for the transverse roll cloud beyond the solitary wave framework. However, an important physical question that has not been discussed so far is how practically these theorems can be realized in the real atmospheric boundary layer. In particular, it is necessary to assess the physical aspects of the criteria for the boundary layer separation as established in Theorem III.1. Specifically, Theorem III.1 explicitly indicates the locations where boundary layer separations may occur, which are given by

$$x_n = \frac{(4n+1)\pi}{2a_k},$$

where $a_k = \frac{k\pi}{\gamma}$ and γ is the ratio of the horizontal scale l of the domain over the vertical depth h. As illustrated in Fig. 5, these locations can roughly be identified as the places where TCRs form inside the domain $[0, l]$ if and only if the location x_n must lie within the domain $[0, \gamma]$, i.e.,

$$x_n = \frac{(4n+1)\pi}{2a_k} < \gamma,$$

which is equivalent to

$$\frac{4n+1}{2k} < 1. \tag{4.1}$$

Here, n denotes the number of vortices associated with the boundary layer separation at the point x_n.

While it may look at first that this condition is purely a function of the domain topology, it should be recalled that k is a function of the critical number R_c and so implicitly encodes the dynamics of the MRB system. A rearrangement of (4.1) gives

$$k > 2n + \frac{1}{2} \geq \frac{5}{2} \text{ for } (n \geq 1) \tag{4.2}$$

or

$$k > 3. \tag{4.3}$$

The constraint (4.3) is important because it can be considered as a requirement that the MRB system must possess such that the physical interpretation of the boundary layer separation as a mechanism for the formation of transverse clouds is plausible.

To see if the condition $k > 3$ is realized in a real atmospheric PBL, we consider a range of typical values for the PBL including the PBL depth $h \sim 1000$ m, $\rho_0 \sim 1$ kg m^{-3}, $p_0 \sim 10^{-5}$ Pa m^{-1}, and $l \sim 100$ km. Given these scales, we obtain $\gamma \sim 100$, $\beta \sim 0.01$. The condition (2.21) then gives $k \sim 85$ with the corresponding critical value $R_c^{\beta} \approx 1100$. For this set of parameters, the requirement $k > 3$ is thus well ensured for the real PBL flow. Note again that in general, γ, k, and R_c^{β} are all constrained by the MRB system (2.14) [see also Eq. (2.21)].

Because of (4.3) and (2.21), it is apparent that the ratio γ should not be too small, i.e., the horizontal scale must be much larger than the vertical depth of the PBL. Otherwise, there would be no vortex separating from boundary. In fact, (4.1) provides an estimation for the number of transverse rolls as a function of k as follows:

$$n = \left[\frac{k}{2} - \frac{1}{4}\right]. \tag{4.4}$$

With $k \sim 85$ as derived above, we have $n \sim \left[\frac{85}{2} - \frac{1}{4}\right] \sim 41$, i.e., there are about 40 cloud rolls within a horizontal domain of 100 km long, which appears to be a good upper bound for the number of transverse cloud rolls in reality.

The second question we need to address is the requirement for Theorem II.1 to be valid. We note again that the proof of this theorem is based on an assumption that $\beta \ll 1$, and the modified Rayleigh number $R \equiv \hat{R}(1+\bar{\lambda})$ must be greater than the critical value R_c^β. Recall from the definitions of these two parameters that

$$\beta = \frac{p_0 h^3}{\rho_0 \nu_E \kappa_E}, \quad R = \frac{g(\theta_0 - \theta_1)h^3}{\theta_0 \nu_E \kappa_E}\left(1 + \frac{h\lambda}{\theta_0 - \theta_1}\right).$$

It is apparent from these expressions for β and R that the requirement of $\beta \ll 1$ and $R > R_c^\beta$ can only be ensured if the horizontal pressure gradient p_0 is sufficiently small, while in the meantime, the temperature gradient $(\theta_0 - \theta_1)$ between $z = 0$ and $z = h$ must be larger than a critical value. Given the typical values of the atmospheric boundary layer with $h \sim 10^3$ m, $\rho_0 \sim 1$ kg m^{-3}, $1/\theta_0 \sim 10^{-2}$ K^{-1}, $\lambda \sim 10^{-3}$, $\nu_E \sim \kappa_E \sim 10^3$ such that the Pratt number $P_r \sim 1$,[39,40] one can see that $\beta < 0.1$ only if $p_0 < 10^{-4}$ Pa m^{-1}, and $R > R_c^\beta \approx 1100$ only if $(\theta_0 - \theta_1) > 10$ K. These requirements for p_0 and $(\theta_0 - \theta_1)$ are again reasonable in the real atmospheric PBL, thus confirming the applicability of the transition dynamics in understanding the formation of transverse roll clouds.

Physically, the requirement on the horizontal pressure gradient p_0 is expected because a too strong pressure gradient in the x-direction would generate a very large shear flow $\bar{u} = \beta f(z)$, which tends to favor the development of longitudinal rolls rather than transversal rolls. Likewise, the vertical temperature gradient must be sufficiently large such that convection can develop, thus promoting the formation of the boundary layer separations that host TCRs. One notices here the subtle contribution of the latent heat release effect, which is represented by the factor λ. Apparently, the inclusion of this latent heating would increase the Rayleigh number by a factor of $(1 + \bar{\lambda})$, thus supporting the TCR development, even with relatively weak shear environment. Other than this shift in the threshold of the Rayleigh number for the boundary layer separation, the latent heat effect associated with cloud formation does not have much impacts on the characteristics of either attractor bifurcation or boundary layer separation processes.

V. CONCLUSION

In this study, the potential mechanisms underlying the formation of transverse cloud rolls (TCRs) in the atmospheric boundary layer were examined in the framework of the dynamical transition. Unlike the traditional approach to the TCR formation that is based on the linear stability analyses, the formation of TCRs is considered in this study as a manifestation of (1) an attractor bifurcation at some critical Rayleigh numbers caused by a sufficiently large vertical gradient of temperature and (2) the boundary layer separation related to the presence of a mean shear flow. The main results derived from these above analyses are summarized as follows (see Theorems II.1 and II.2):

(1) In the absence of vertical wind shear (i.e., $\beta = 0$), there does not exist any boundary layer separation process in the system (2.8). In this case, the attractor bifurcation given in Theorems II.1 and II.2 is essentially the classical Rayleigh-Bénard convection, with the Rayleigh number modified by a factor proportional to latent heating during cloud formation;
(2) In the presence of weak vertical wind shear $\beta \neq 0$ and $\beta \ll 1$, there exists $R_1 > R_c^\beta$ such that (2.8) exhibits the boundary layer separation at $R = R_1$. The ascending branches at the stagnation points are linked to the TCR formation;
(3) For fixed β, if $R < R_1$, the topological structure of flow is a purely horizontal shear flow, as shown in Fig. 2, whereas for $R > R_1$, a new topological structure of the total flows, as shown in Fig. 7, will develop, which describe the transverse cloud rolls.

While the dynamics of TCRs contains many intricate features related to nonlinearity feedback between dynamic and thermodynamic processes, our proposed model for the transverse rolls based on a modified version of the Rayleigh-Bénard convection model could reveal a number of important features related to the transverse roll formation. Specifically, by taking into account the effect of latent heat release, explicit criteria for the TCR formation were obtained from the modified Rayleigh-Bénard convection model. These criteria allow for calculation of the number of transverse rolls as a function of the domain ratio γ, the wind shear magnitude β, the gradient of the horizontal pressure p_0, and the vertical gradient of potential temperature $\theta_1 - \theta_0$. The number of transverse rolls turns out to be very sensitive to these parameters and may lead to no transverse cloud rolls even when the system (2.10) undergoes an attractor bifurcation. Specifically, the following two conditions must satisfy so that the TCR formation can occur:

$$\hat{R} = \frac{g(\theta_0 - \theta_1)h^3}{\theta_0 \nu_E \kappa_E}\left(1 + \frac{h\lambda}{\theta_0 - \theta_1}\right) > 1100$$

and

$$\beta = \frac{p_0 H^3}{\rho_0 \nu_E \kappa_E} \ll 1.$$

These two conditions, in conjunction with the criterion for a countable number of transverse rolls within a given domain as shown by Eq. (4.4), can be used to directly examine the validity of our transverse roll cloud model in future.

ACKNOWLEDGMENTS

This research is supported in part by the Indiana University Faculty Research fund and by the Office of Naval Research (ONR)'s Young Investigator Program Award. The first author wishes to acknowledge the support from the National Natural Science Foundation of China (NSFC), Grant No. 11901408. The authors wish to thank two reviewers for their constructive comments and suggestions, which have helped improve this work substantially.

APPENDIX: PROOFS OF MAIN THEOREMS

Proof of Theorem II.1 and Theorem II.2. We shall use results presented in Ref. 27 to prove the above two theorems. In fact, we only need to verify that the MRB system satisfies the necessary conditions of the main theorems about the attractor bifurcation in Ma and Wang's boundary layer separation theorems.[27] To this end, (2.10) is first rewritten in the form of operator equation as follows:

$$\frac{d\mathbf{v}}{dt} = L_R\mathbf{v} + S_\beta\mathbf{v} + G(\mathbf{v}), \mathbf{v} = (u, w, \theta), \tag{A1}$$

where the operators L_R, S_β, and G are defined as

$$L_R = A + \sqrt{R}B, \tag{A2}$$

$$A\mathbf{v} = (\mathbb{P}[P_r\Delta u, P_r\Delta w], \theta), B\mathbf{v} = [\mathbb{P}(0, P_r\theta), w], \tag{A3}$$

$$S_\beta\mathbf{v} = \left(\mathbb{P}\left[-\beta(z - \frac{z^2}{2})\frac{\partial u}{\partial x} - \beta(1-z)w, -\beta(z-\frac{z^2}{2})\frac{\partial w}{\partial x}\right], -\beta(z-\frac{z^2}{2})\frac{\partial\theta}{\partial x}\right), \tag{A4}$$

$$G(\mathbf{v}, \mathbf{v}) = -(\mathbb{P}[(\mathbf{u}\cdot\nabla)u, (\mathbf{u}\cdot\nabla)w], (\mathbf{u}\cdot\nabla)\theta), \tag{A5}$$

in which $\mathbb{P}$ is the Leray projection. Direct verification of the above operators shows that L_R, S_β, and G satisfy the attractor bifurcation conditions in Ma and Wang's boundary separation theorem. Furthermore, L_R is symmetric and

$$\left(G(\mathbf{v}, \mathbf{v}^*), \mathbf{v}^*\right) = 0,$$

where $G(\mathbf{v}, \mathbf{v}^*)$ is defined from (A5) as

$$G(\mathbf{v}, \mathbf{v}^*) = -\left(P_L\left((\mathbf{u}\cdot\nabla)u^*, (\mathbf{u}\cdot\nabla)w^*\right), (\mathbf{u}\cdot\nabla)\theta^*\right).$$

Because it is known from the results in Ref. 25 that $\mathbf{0}$ is an asymptotically stable steady state of the linear part given by

$$\frac{d\mathbf{v}}{dt} = L_R\mathbf{v} + G(\mathbf{v})$$

at $R = R_0$, the MRB system (2.10) satisfies all conditions of Ma and Wang's theorem. As a result, Theorems II.1 and II.2 follow directly from Ma and Wang's theorem as stated.

Proof of Theorem III.1. From Theorem II.2, it is known that as $R > R_c^\beta$, (2.10) bifurcates from (0, 0) to two other globally stable solutions together with corresponding shear flows given by

$$(\tilde{u}, 0) + \mathbf{u}_{R,i}^\beta, \quad i = 1, 2.$$

Note that, for $b(\beta)$ satisfying $\lim_{\beta\to 0} b(\beta) = 0$, Theorem III.1 will be proven if we can show that there exists a structural bifurcation for the following two vectors:

$$\mathbf{V}_{R,1} \equiv (\beta f(z), 0) + \frac{\sqrt{b^2(\beta) + 4a(R,\beta)} - |b(\beta)|}{2c(\beta)}\overline{\mathbf{W}},$$

$$\mathbf{V}_{R,2} \equiv (\beta f(z), 0) - \frac{\sqrt{b^2(\beta) + 4a(R,\beta)} + |b(\beta)|}{2c(\beta)}\overline{\mathbf{W}},$$

where

$$\overline{\mathbf{W}} = \left(\frac{1}{a_k}\sin a_k x U'(z), -\cos a_k x U(z)\right), \tag{A6}$$

and $U(z)$ is given by (2.17). We now prove the first part of this theorem. Indeed for simplicity, let

$$\delta = \frac{\sqrt{b^2(\beta) + 4a(R,\beta)} - |b(\beta)|}{2a_k c(\beta)}. \tag{A7}$$

δ is an increasing function of R with $\delta = 0$ at $R = R_c^\beta$. Detailed calculations give

$$\frac{\partial\mathbf{V}_{R,1}}{\partial\mathbf{n}} = \frac{\partial\mathbf{V}_{R,1}}{\partial z}\bigg|_{z=0} = \left(\beta + \delta\sin a_k x U''(0), 0\right). \tag{A8}$$

Hence, the condition $\frac{\partial\mathbf{V}_{R,1}}{\partial\mathbf{n}} = 0$ is equivalent to

$$\frac{\beta}{U''(0)} + \delta\sin(a_k x) = 0. \tag{A9}$$

Let $\delta_0 = -\frac{\beta}{U''(0)}$, we then have

$$\frac{\partial\mathbf{V}_{R,1}}{\partial\mathbf{n}}\bigg|_{\left(\frac{(4n+1)\pi}{2a_k}, 0\right)} \begin{cases} \neq 0, & \delta < \delta_0, \\ = 0, & \delta = \delta_0. \end{cases} \tag{A10}$$

The first part of Theorem III.1 is therefore true by simply applying the structural bifurcation Theorems 5.3.6 and 5.3.7 in Ref. 45. That is, we need to verify conditions (5.3.4)–(5.3.7) in the work of Ma and Wang.[45] To verify these conditions in Ref. 45, we employ the Taylor expansion of $\mathbf{V}_{R,1}$ at $\delta = \delta_0$ as follows:

$$\begin{aligned} \mathbf{V}_{R,1} &= \mathbf{V}_{R,1}^0 + (\delta - \delta_0)\mathbf{V}_{R,1}^1, \\ \mathbf{V}_{R,1}^0 &= \left(\delta_0\sin a_k x U'(z) + \beta f(z), -a_k\delta_0\cos a_k x U(z)\right), \\ \mathbf{V}_{R,1}^1 &= \left(\sin a_k x U'(z), -a_k\cos a_k x U(z)\right). \end{aligned} \tag{A11}$$

One can deduce from (2.19) that $U''(0) \approx -24.7808$.

More detailed calculations give

$$\begin{aligned} \frac{\partial\mathbf{V}_{R,1}^0}{\partial\mathbf{n}}\bigg|_{\left(\frac{(4n+1)\pi}{2a}, 0\right)} &= \frac{\partial\mathbf{V}_{R,1}^0}{\partial z}\bigg|_{\left(\frac{(4n+1)\pi}{2a}, 0\right)} = (0, 0), \\ \frac{\partial\mathbf{V}_{R,1}^1}{\partial\mathbf{n}}\bigg|_{\left(\frac{(4n+1)\pi}{2a}, 0\right)} &= \frac{\partial\mathbf{V}_{R,1}^1}{\partial z}\bigg|_{\left(\frac{(4n+1)\pi}{2a}, 0\right)} = (-24.7808, 0), \\ \frac{\partial^3\left(\mathbf{V}_{R,1}^0\cdot\tau\right)}{\partial\tau^2\partial\mathbf{n}}\bigg|_{\left(\frac{(4n+1)\pi}{2a}, 0\right)} &= \frac{\partial^3\left(\mathbf{V}_{R,1}^0\cdot\tau\right)}{\partial x^2\partial z}\bigg|_{\left(\frac{(4n+1)\pi}{2a}, 0\right)} \\ &= 24.7808a^2\delta_0. \end{aligned}$$

As a result, all conditions (5.3.4), (5.3.6), and (5.3.7) in Theorem 5.3.6 and 5.3.7 in Ma and Wang[45] are realized. To verify the last condition (5.3.5) in Ma and Wang's theorem, i.e.,

$$\text{Index}\left(\frac{\partial\mathbf{V}_{R,1}}{\partial z}\left(\frac{(4n+1)\pi}{2a}, 0\right)\right) = 0, \tag{A12}$$

we only need to check that the equation

$$\frac{\partial(\mathbf{V}_{R,1}\cdot\tau)}{\partial z} = \delta\sin a_k x U''(z) + \beta(1-z) = 0 \tag{A13}$$

has no solution on $\delta < \delta_0$ in a small neighborhood of $\left(\frac{(4n+1)\pi}{2a_k}, 0\right)$ due to the invariance of the index sum of singular points in a domain. Take the Taylor expansion of $U''(z)$ at $z = 0$ as follows:

$$U''(z) = U''(0) + U'''(0)z + o(z),$$
$$U''(0) \approx -24.7808, U'''(0) \approx 139.977;$$

then (A13) can be rewritten as

$$\delta \sin a_k x\left(U''(0) + U'''(0)z\right) + \beta(1 - z) + o(z) = 0,$$

which is equivalent to

$$\frac{\delta}{\delta_0} \sin a_k x - 1 + \left(\frac{-139.977\delta}{\beta} \sin a_k x + 1\right)z + o(z) = 0. \quad \text{(A14)}$$

If $\delta < \delta_0$, we know from (A14) that there exists a small neighborhood Ω_s of $\left(\frac{(4n+1)\pi}{2a}, 0\right)$ in which (A14) has no solution. Then condition (5.3.5) also holds true. Let R_1 be the number such that $\delta(R_1) = \delta_0$. Using (A10) gives that $R_1 > R_c^\beta$. Therefore, from Theorems 5.3.6 and 5.3.7 in Ref. 45, we know that the MRB system (2.10) has a structural bifurcation at $R = R_1 > R_c^\beta$.

With the above conditions ensured, the first assertion of Theorem III.1 is valid if we can finally show that the vector field $\mathbf{V}_{R,1}$ has no inner singular points for $R_c^\delta < R < R_1$, while it has a unique singular point in each domain $\left(\frac{(2n+1)\pi}{a_k}, \frac{(2n+2)\pi}{a_k}\right) \times (0, 1)$ for $R > R_1$. From $U(z) < 0$ in (0,1), we see that the singular point is $\left(\frac{(4n+1)\pi}{2a_k}, z\right)$, where z is determined by the solution of the following equation:

$$F(z) = \left(z - \frac{z^2}{2}\right) + \frac{\delta}{\beta}U'(z) = 0. \quad \text{(A15)}$$

In fact, for $\delta > \delta_0 = \frac{\beta}{-U''(0)}$, we have

$$F'(z)|_{z=0} = 1 + \frac{\delta}{\beta}U''(0) < 1 + \frac{\delta_0}{\beta}U''(0) = 0, \quad \text{(A16)}$$

which means (A15) has a unique solution in (0, 1). Thus, the first assertion of Theorem 3 is proven.

For the second assertion, let $b_0 = a_k c(\beta)\frac{\beta}{U''(0)}$ and denote

$$\delta^* = \frac{\sqrt{b^2(\beta) + 4a(R,\beta)} + |b(\beta)|}{2a_k c(\beta)}; \quad \text{(A17)}$$

one gets that

$$\delta_0 = \frac{\beta}{-U''(0)} > \delta^*(R_c^\beta), \quad \text{(A18)}$$

for the case of $|b(\beta)| < b_0$. Let R_2 be the number such that $\delta^*(R_2) = \delta_0$. Then, similar to the proof of assertion (1), part one of assertion (2) holds true. If $|b(\beta)| > b_0$, in a similar way, one can prove that vector field $\mathbf{V}_{R,2}$ has no inner singular points for $R < R_2$, while it has a unique singular point in each domain $\left(\frac{(2n+1)\pi}{a}, \frac{(2n+2)\pi}{a}\right) \times (0, 1)$ on $R > R_2$. This proves the second assertion. Given assertions (1) and (2), the last assertion of the theorem thus follows naturally as a combination of assertions (1) and (2).

REFERENCES

[1] F. H. Busse, "Transition to turbulence in Rayleigh-Bénard convection," in *Hydrodynamic Instabilities and the Transition to Turbulence*, Topics in Applied Physics Vol. 45 (Springer, Berlin, 1985), pp. 97–137.
[2] R. A. Brown, "Longitudinal instabilities and secondary flows in planetary boundary layer," Rev. Geophys. **18**, 683–697, https://doi.org/10.1029/rg018i003p00683 (1980).
[3] J. P. Kuettner, "The band structure of the atmosphere," Tellus **11**, 267–294 (1959).
[4] S. Chandrasekhar, *Hydrodynamic and Hydromagnetic Stability* (Courier Corporation, 2013).
[5] H. Jeffreys, "The stability of a layer of fluid heated below," London, Edinburgh, Dublin Philos. Mag. J. Sci. **2**, 833–844 (1926).
[6] V. Iudovich, "Free convection and bifurcation," J. Appl. Math. Mech. **31**, 103–114 (1967).
[7] T. Asai, "Three dimensional features of thermal convection in a plane Couette flow," J. Meteorol. Soc. Jpn., Ser. II **48**, 18–29 (1970).
[8] R. M. Clever and F. H. Busse, "Three dimensional convection in a horizontal fluid layer subjected to a constant shear," J. Fluid Mech. **234**, 511–527 (1992).
[9] R. M. Clever and F. H. Busse, "Instabilities of longitudinal rolls in the presence of Poiseuille flow," J. Fluid Mech. **229**, 517–529 (1992).
[10] P. Carrière and P. A. Monkewitz, "Convective versus absolute instability in mixed Rayleigh-Bénard-Poiseuille convection," J. Fluid Mech. **384**, 243–262 (1999).
[11] Y. Miura, "Aspect ratios of longitudinal rolls and convections cells observed during cold air outbreak," J. Atmos. Phys. **43**, 26–39 (1986).
[12] R. C. Hathaway and J. Sommerville, "Thermal convection in a rotating shear flow," J. Fluid Mech. **38**, 43–68 (1987).
[13] R. A. Brown, "A secondary flow model for planetary boundary layer," J. Atmos. Sci. **27**, 742–757 (1970).
[14] D. Etling and R. A. Brown, "Roll vortices in the planetary boundary layer: A review," Boundary-Layer Meteorol. **65**, 215–248 (1993).
[15] H. L. Kuo, "Perturbations of plane Couette flow in stratified fluid and origin of cloud sheets," Phys. Fluids **6**, 195–211 (1963).
[16] J. P. Kuettner, "Cloud bands in the earth's atmosphere: Observations and theory," Tellus **23**, 404–426 (1971).
[17] R. Kelly, "The onset and development of thermal convection in fully developed shear flows," Adv. Appl. Mech. **31**, 35–112 (1994).
[18] M. Akiyama, G. J. Hwang, and C. K. Cheng, "Experiments on the onset of longitudinal vortices in laminar forced convection between horizontal plates," J. Heat Transfer **93**, 335–341 (1971).
[19] K. Fukui, M. Nakajima, and H. Huena, "The longitudinal vortex and its effects on the transport processes in combined free and forced laminar convection between horizontal and inclined parallel plates," Int. J. Heat Mass Transfer **26**, 109–120 (1983).
[20] S. Ostrach and Y. Kamotani, "Heat transfer augmentation in laminar fully developed channel flow by means of heating from below," J. Heat Transfer **97**, 220–225 (1975).
[21] J.-M. Luijkx, J. K. Platten, and J. C. Legros, "On the existence of thermoconvective rolls, transverse to a superimposed mean Poiseuille flow," Int. J. Heat Mass Transfer **24**, 1287–1291 (1981).
[22] H. W. Muller, M. Lucke, and M. Kamps, "Transversal convection patterns in horizontal shear flow," Phys. Rev. A **45**, 3714–3726 (1992).
[23] M. T. Ouazzani, J. K. Platten, and A. Mojtabi, "Experimental study of mixed convection between two horizontal plates at different temperatures," Int. J. Heat Mass Transfer **33**, 1417–1427 (1990).
[24] H. W. Muller, M. Tveitereid, and S. Trainoff, "Rayleigh-Bénard problem with imposed weak through-flow: Two coupled Ginzburg-Landau equations," Phys. Rev. E **48**, 263–272 (1993).
[25] T. Ma and S. Wang, "Attractor bifurcation theory and its applications to Rayleigh-Bénard convection," Commun. Pure Appl. Anal. **2**, 591–599 (2003).
[26] T. Ma and S. Wang, "Dynamic bifurcation and stability in the Rayleigh-Bénard convection," Commun. Math. Sci. **2**, 159–183 (2004).
[27] T. Ma and S. Wang, *Phase Transition Dynamics* (Springer, 2013), p. 555.

[28]T. Ma and S. Wang, *Bifurcation Theory and Applications*, World Scientific Series on Nonlinear Science. Series A: Monographs and Treatises Vol. 53 (World Scientific Publishing Co. Pte. Ltd., Hackensack, NJ, 2005).
[29]M. E. Tern, *Ocean Circulation Physics* (Academic Press, New York, 1975), p. 246.
[30]T. Ma and S. Wang, "Stability and bifurcation of the Taylor problem," Arch. Ration. Mech. Anal. **181**, 149–176 (2006).
[31]T. Ma and S. Wang, "Boundary-layer and interior separations in the Taylor–Couette–Poiseuille flow," J. Math. Phys. **50**, 033101 (2009).
[32]Q. Wang, H. Luo, and T. Ma, "Boundary layer separation of 2-D incompressible Dirichlet flows," Discrete Contin. Dyn. Syst., Ser. B **20**, 675–682 (2015).
[33]H. Luo, Q. Wang, and T. Ma, "A predicable condition for boundary layer separation of 2-D incompressible fluid flows," Nonlinear Anal.: Real World Appl. **22**, 336–341 (2015).
[34]C. Lu, Y. Mao, Q. Wang, and D. Yan, "Hopf bifurcation and transition of three-dimensional wind-driven ocean circulation problem," J. Differ. Equations **267**, 2560–2593 (2019).
[35]D. Han, M. Hernandez, and Q. Wang, "Dynamic bifurcation and transition in the Rayleigh-Bénard convection with internal heating and varying gravity," Commun. Math. Sci. **17**, 175–192 (2019).
[36]C. Kieu, T. Sengul, Q. Wang, and D. Yan, "On the Hopf (double Hopf) bifurcations and transitions of two-layer western boundary currents," Commun. Nonlinear Sci. Numer. Simul. **65**, 196–215 (2018).
[37]R. Liu and Q. Wang, "S^1 attractor bifurcation analysis for electrically conducting fluid flows between two concentric axial cylinders," Physica D **392**, 17–33 (2019).
[38]T. Ma and S. Wang, "Rayleigh-Bénard convection: Dynamics and structure in the physical space," Commun. Math. Sci. **5**, 553–574 (2007).
[39]A. Malhotra and S. S. Kang, "Turbulent Prandtl number in circular pipes," Int. J. Heat Mass Transfer **27**, 2158–2161 (1984).
[40]I. Takahiro and O. Hisao, "Theory of eddy viscosity coefficient for two-dimensional inviscid barotropic fluid," Prog. Theor. Phys. **90**, 1229–1240 (1993).
[41]M. Ghil, T. Ma, and S. Wang, "Structural bifurcation of 2-D incompressible flows," Indiana Univ. Math. J. **50**, 159–180 (2001).
[42]M. Ghil, J.-G. Liu, C. Wang, and S. Wang, "Boundary-layer separation and adverse pressure gradient for 2-D viscous incompressible flow," Physica D **197**, 149–173 (2004).
[43]T. Ma and S. Wang, "Boundary layer separation and structural bifurcation for 2-D incompressible fluid flows," Discrete Contin. Dyn. Syst. **10**, 459–472 (2004).
[44]T. Ma and S. Wang, "Rigorous characterization of boundary layer separations," in Proceedings of the Second MIT Conference on Computational Fluid and Solid Mechanics, Cambridge, MA, 2003.
[45]T. Ma and S. Wang, "Geometric theory of incompressible flows with applications to fluid dynamics," AMS Math. Surv. Monogr. Ser. **119**, 234 (2005).